Supporting information for

Synthesis modulation as a tool to increase the catalytic activity of MOFs: the unique case of UiO-66(Zr)

Frederik Vermoortele[a], Bart Bueken[a], Gaëlle Le Bars[b], Ben Van de Voorde[a], Matthias Vandichel[c], Kristof Houthoofd[a], Alexandre Vimont[b], Marco Daturi[b], Michel Waroquier[c], Veronique Van Speybroeck[c], Christine Kirschhock[a], Dirk E. De Vos[a]

[a] Centre for Surface Chemistry and Catalysis, Katholieke Universiteit Leuven
[b] Laboratoire Catalyse et Spectrochimie, ENSICAEN, Université de Caen, CNRS
[c] Center for Molecular Modeling, Universiteit Gent

MOF synthesis and characterization

All chemicals and solvents used in the syntheses were of reagent grade and used without further purification.

All materials were made in a closed Schott DURAN® pressure plus bottle with a volume of 1 l under static conditions, starting from an equimolar solution of $ZrCl_4$ (3.5 g, 15 mmol) and terephthalic acid (2.5 g, 15 mmol) dissolved in DMF (155 ml, 2 mol). When HCl was used, 1.5 ml of a 36 wt% solution of HCl (17 mmol) was added. In the modulated synthesis, 10-20 equivalents (respectively 11.5 ml and 23 ml of CF_3COOH) were also added to the mixture.

All synthesis mixtures were placed in a preheated oven at 120°C for 21 h. The powders were collected *via* centrifugation and thoroughly washed with DMF (3 times) and methanol (3 times).

^{19}F-NMR

The ^{19}F MAS NMR spectra were recorded on a Bruker Avance DSX400 spectrometer (9.4 T). 352 scans were accumulated with a recycle delay of 60 s. The pulse length was 5.0 μs. The samples were packed in 4 mm rotors; the spinning frequency of the rotor was 10 kHz. CF_3COOH (Acros Organics) was used as chemical shift reference (δ = –76.55 ppm with respect to $CFCl_3$).

XRD

X-ray diffractograms were routinely collected on a Stoe COMBI P diffractometer (λ = 1.54056 Å). Diffractograms of the materials with increasing amounts of modulator are shown in Figure S1. A comparison of the high resolution X-ray diffractograms, collected on a Stoe Stadi MP diffractometer (λ = 1.54056 Å), of UiO-66-10_{HCl} treated at 200 and 320°C is given in Figure S2.

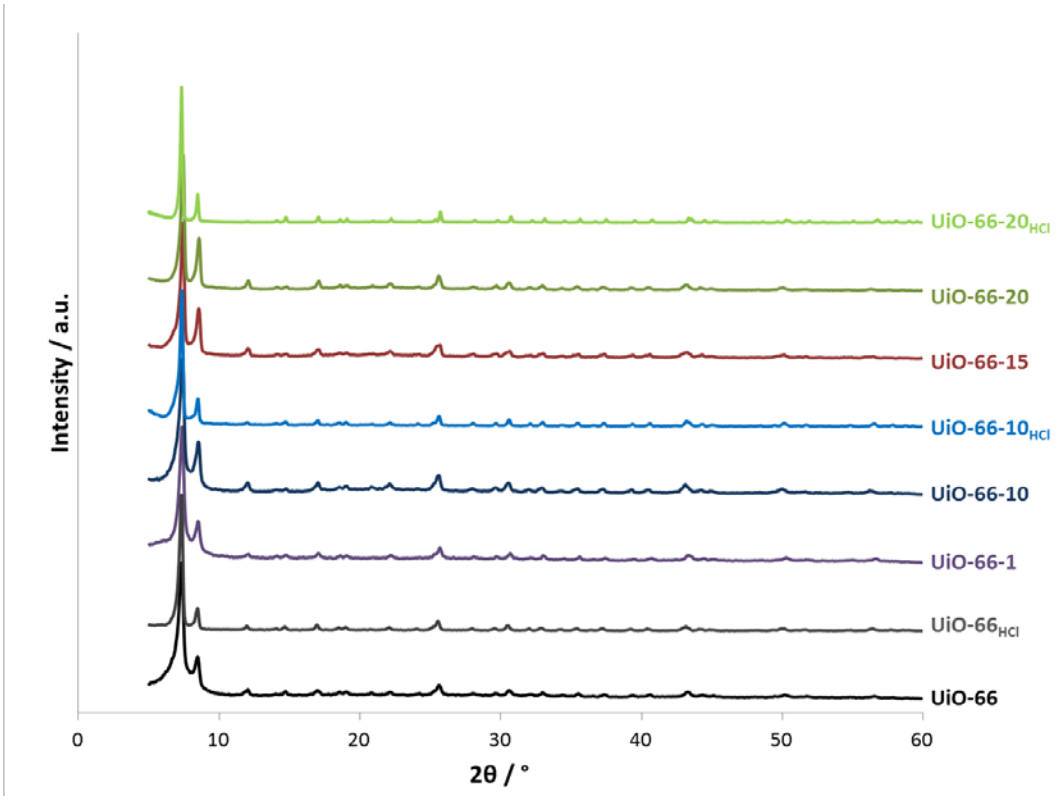

Figure S1. X-ray diffractograms of UiO-66-X synthesized with increasing amounts of TFA, in the presence or absence of HCl.

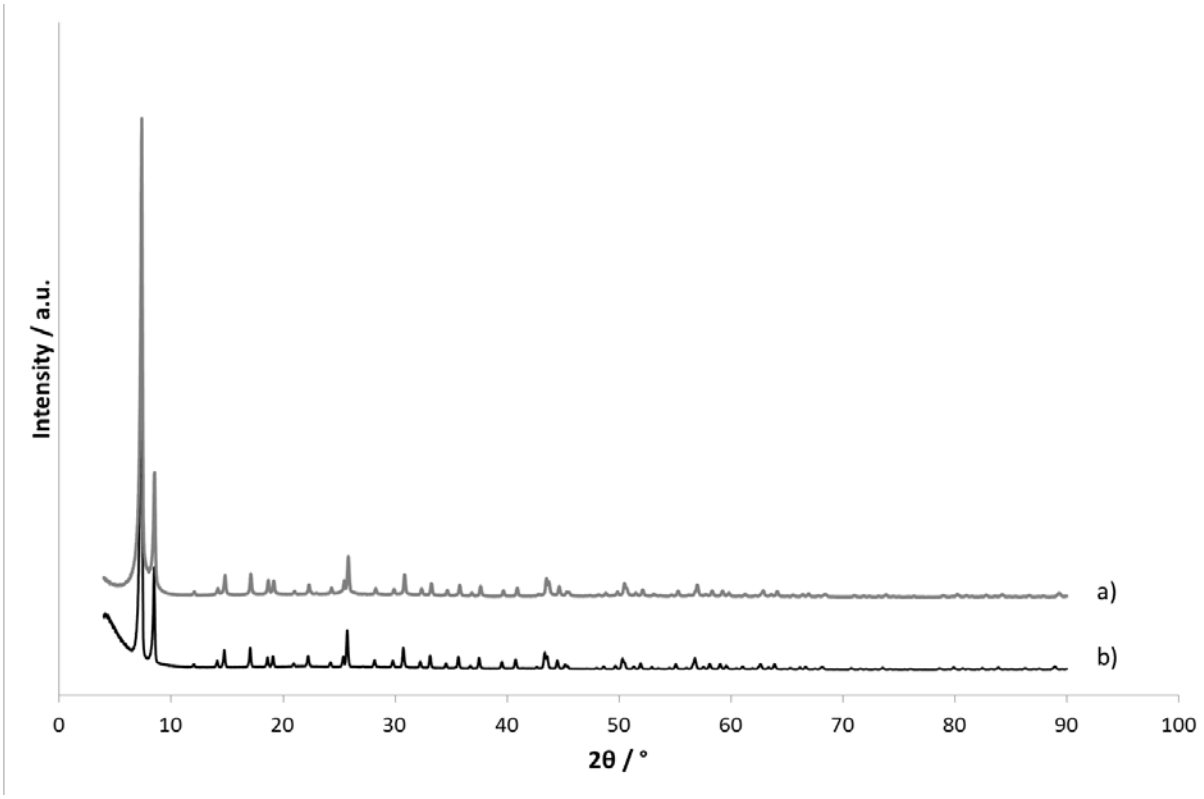

Figure S2. High-resolution X-ray diffractograms of (a) UiO-66-10_{HCl} activated at 320°C, (b) UiO-66-10_{HCl} activated at 200°C.

SEM

SEM images were obtained using a Philips XL 30 FG.

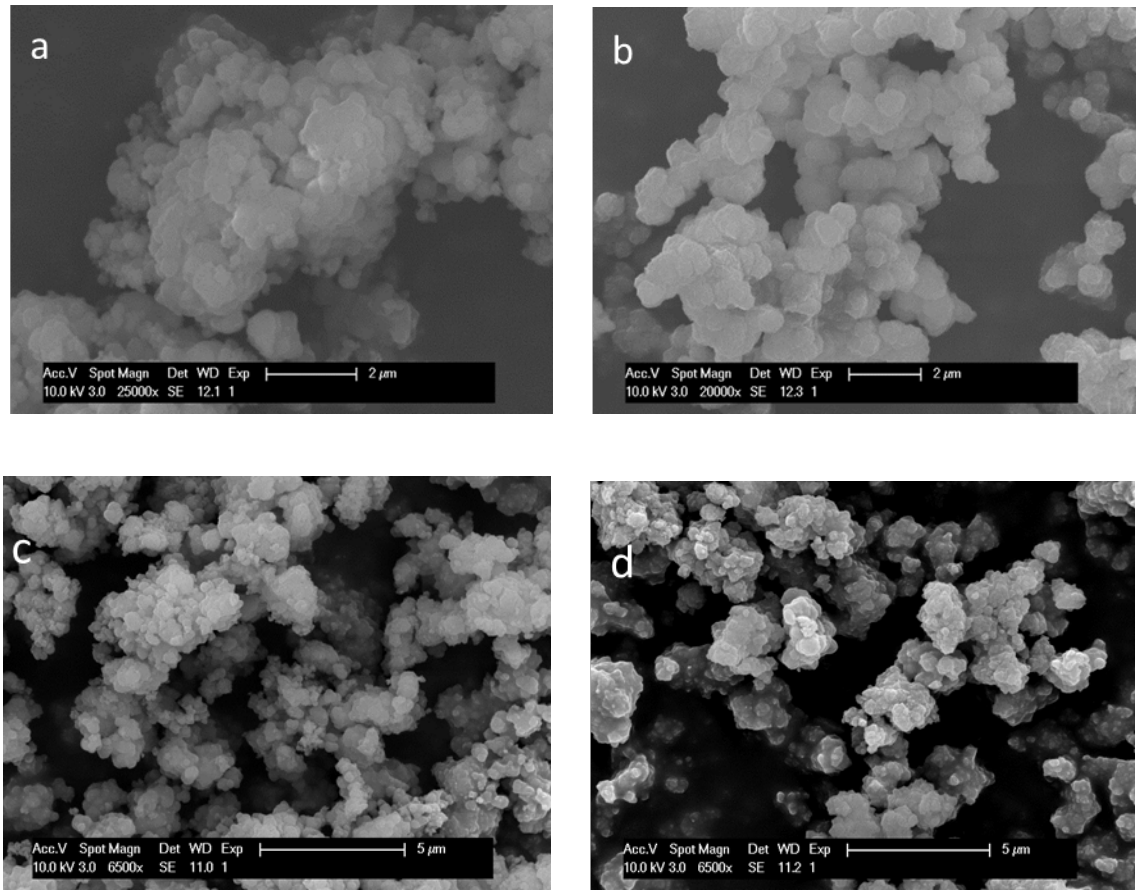

Figure S3. SEM pictures of (a) UiO-66_{HCl}; (b) UiO-66-10_{HCl}; (c) UiO-66 and (b) UiO-66-10.

EDX

EDX spectra of UiO-66-10_{HCl} and UiO-66_{HCl} were measured on a Philips XL 30 FG, equipped with an EDAX EDX system.

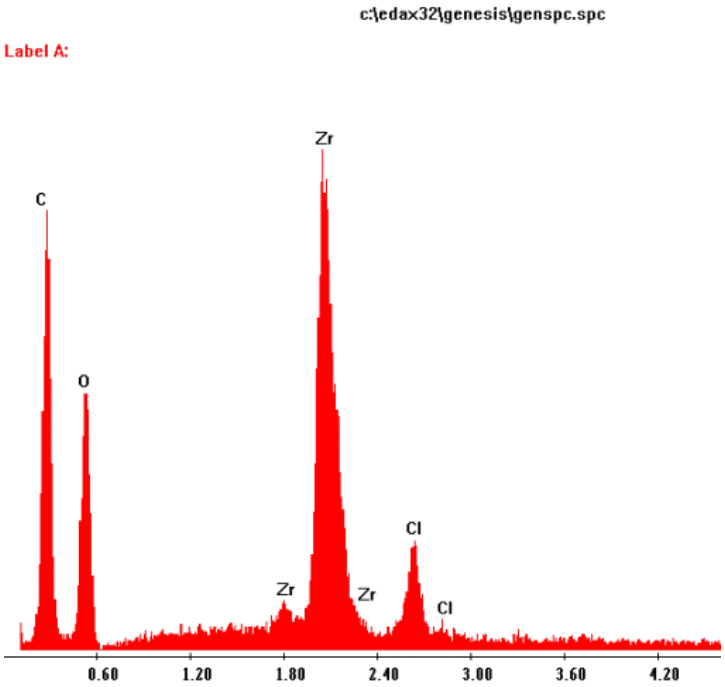

Figure S4. EDX spectrum of UiO-66

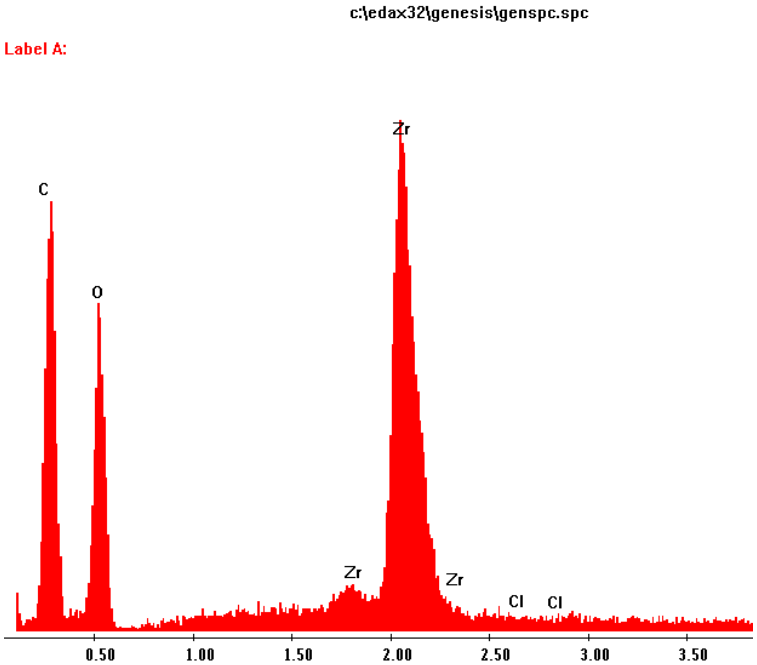

Figure S5. EDX spectrum of UiO-$66_{10,HCl}$

TGA

Thermogravimetric analyses were performed (on a TQA 500 of TA Instruments) to analyze the linker deficiency of each material. Measurements were performed by heating the samples at 3°C / min under an oxygen containing atmosphere. Weights were normalized with respect to the ZrO_2 residue left after heating up to 500°C.

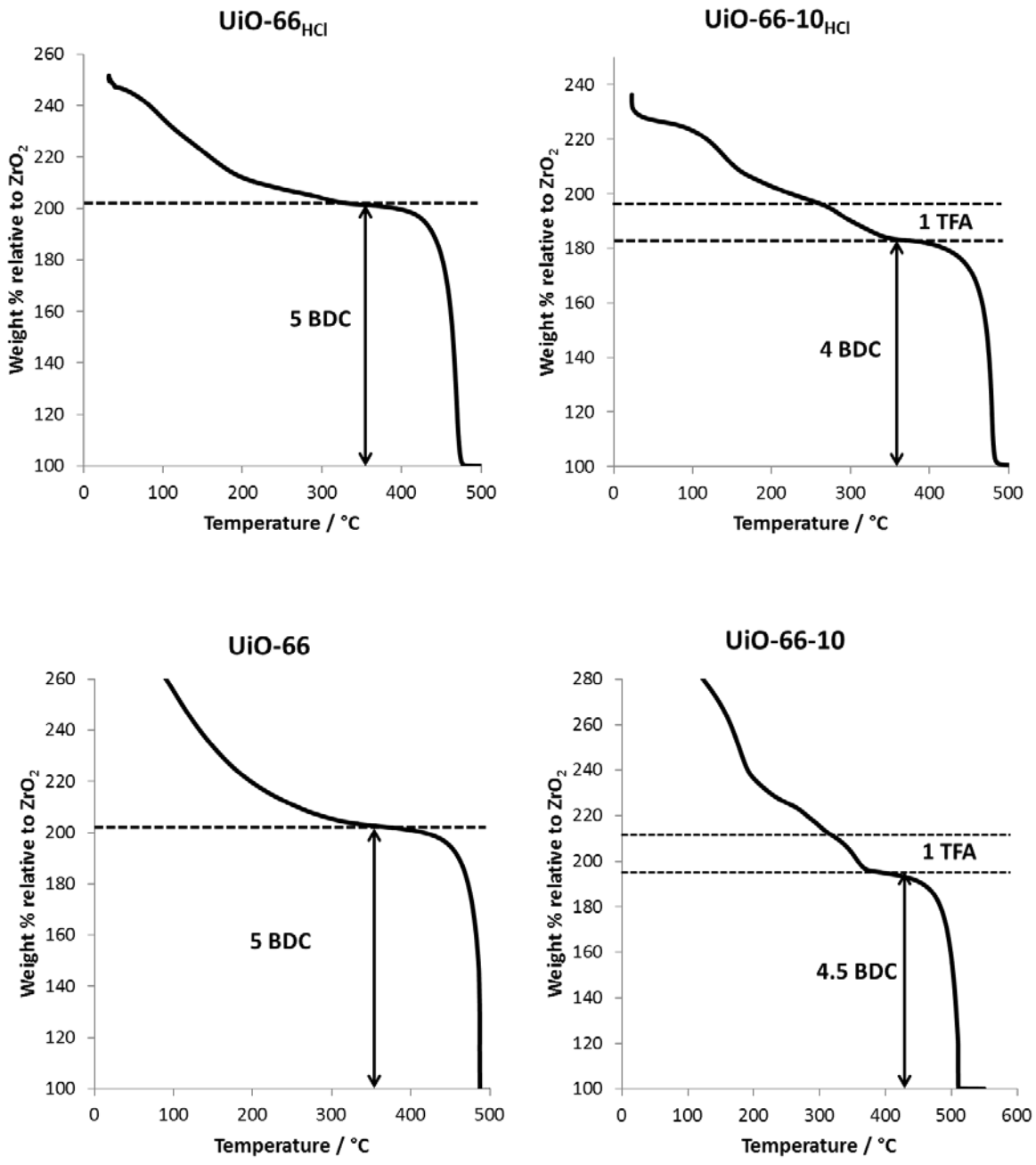

Figure S6. TGA curves of (top left) UiO-66_{HCl} , (top right) UiO-66-10_{HCl} ,(bottom left) UiO-66 and (bottom right) UiO-66-10, indicating the weight loss corresponding to different amounts of carboxylates.

FTIR – CD_3CN chemisorption

Transmission IR spectra were recorded, at 4 cm^{-1} resolution, on a Nicolet Nexus spectrometer equipped with an extended KBr beam splitting device and a MCT cryo-detector. The samples were activated *in situ* prior to the CD_3CN chemisorption experiments.

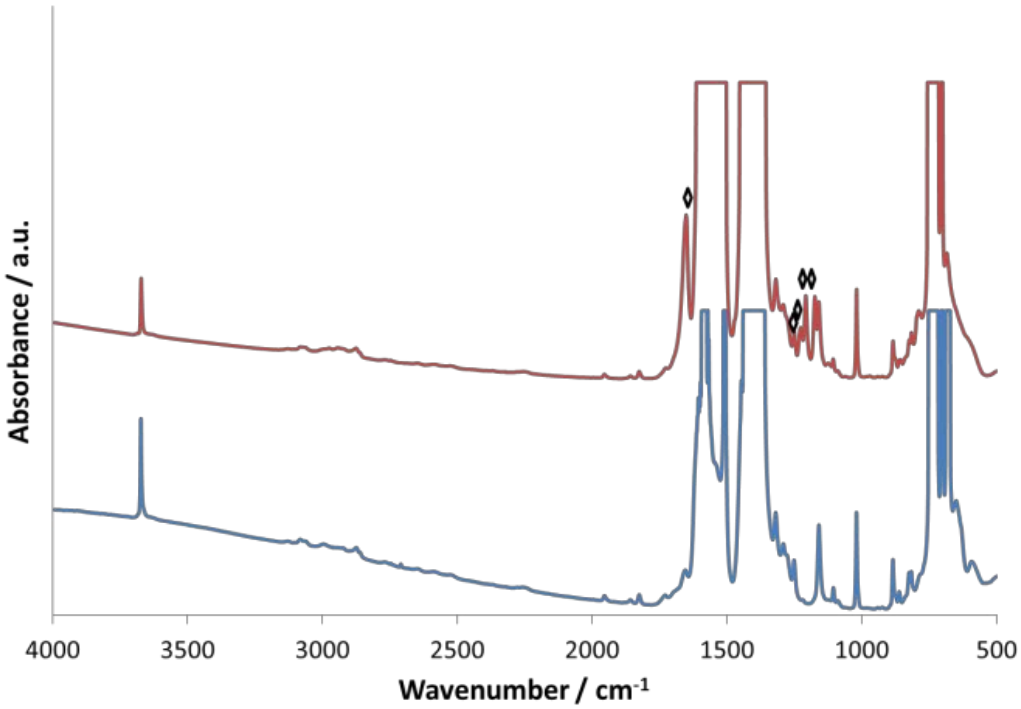

Figure S7. Normalized FTIR spectra of UiO-66_{HCl} (blue) and UiO-66-10_{HCl} (red) at 150°C. Diamonds indicate typical vibrational signals for trifluoroacetate.

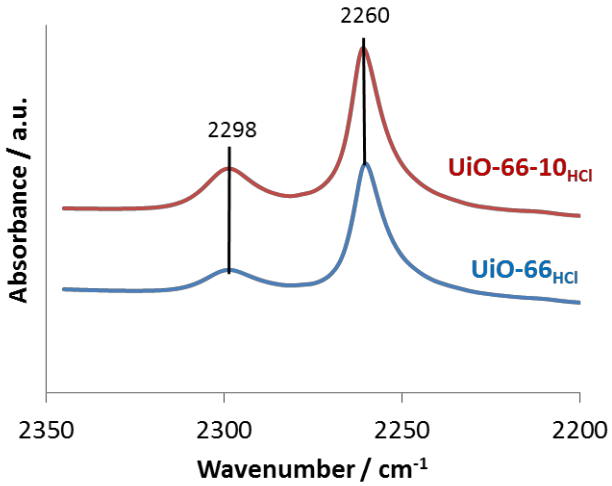

Figure S8. Normalized FTIR-spectra of CD_3CN chemisorption at 53 mbar on UiO-66-10_{HCl} and UiO-66_{HCl}.

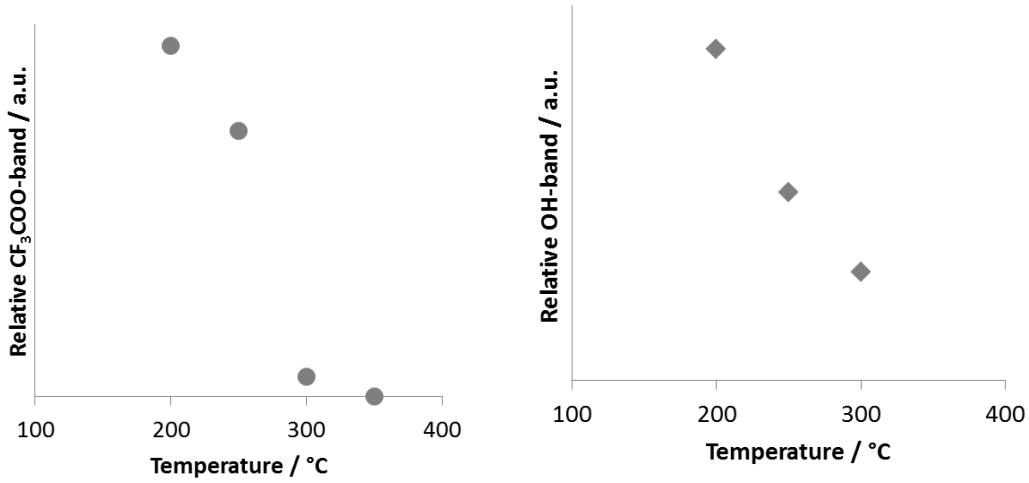

Figure S9. Relative area of (left) the CF_3COO-band at 1208 cm^{-1} and (right) OH-band at 3670 cm^{-1} as a function of activation temperature in UiO-66-10_{HCl}.

Pore size distributions

Nitrogen physisorption was measured using a Quantachrome instrument. Pore size distributions were calculated using a DFT method embedded in the software.

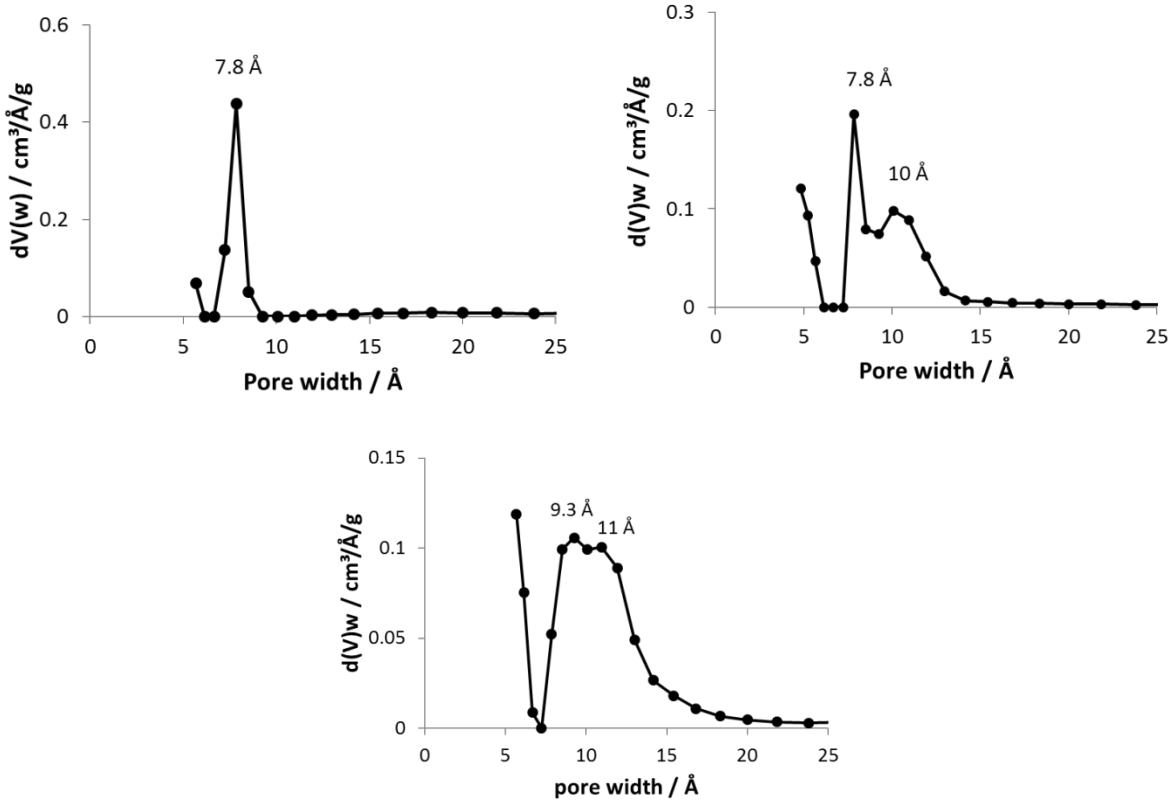

Figure S10. Pore size distributions of (top left) UiO-66_{HCl}, (top right) UiO-66-10_{HCl} and (bottom) UiO-66-20_{HCl}.

Procedures for catalytic test reactions

Before reaction, each catalyst was dried at 320 °C to remove residual solvent molecules. Catalytic reactions were carried out in 10 ml glass crimp cap reactors loaded with 50 mg catalyst and a magnetic stirring bar.

Citronellal cyclization

To the 10 ml glass reactors containing the MOF, a solution of citronellal in 5 ml toluene was added. For each catalyst, a citronellal to Zr ratio of 15 was used. After introduction of the reaction mixture, the vessels were placed in an aluminium heating block at 110°C and stirred. Reaction samples were filtered through a 0.2 µm filter and analyzed with a Shimadzu 2010 GC equipped with a FID detector and a DB-FFAP column.

Meerwein-Ponndorf-Verley reduction

To the 10 ml glass reactors containing the MOF, 10 ml of a solution containing 4-*tert*-butylcyclohexanone (TCH) and isopropylalcohol (IPA) is added. The molar ratio in the reaction mixture is IPA/TCH/Zr^{4+} = 50/10/1. A typical reaction solution for UiO-66 contains 0.183 M TCH and 0.915 M IPA in toluene; n-decane is added as an internal standard. The reaction is performed at 100°C in an aluminium heating block equipped with a stirrer. Reaction samples were filtered through a 0.2 µm filter and analyzed with a Shimadzu 2010 GC equipped with a FID detector and a CP-Sil-8 CB column.

Screening of monocarboxylic acids

We assessed the influence of several monocarboxylic acids used during the synthesis of UiO-66 on the activity of these materials in the citronellal cyclization. Conversions after 10 h are compared. From the table, it is clear that the use of trifluoroacetic acid produces the material with the highest activity.

Table S1. Screening of influence of monocarboxylic acid modulator on the catalytic activity in the citronellal cyclization.

Modulator	**pK_a**	**Conversion at 10 h (%)**	***k*** **(h^{-1})**	***k_{rel}***
trifluoroacetic acid	~0	**61**	0.183	**2.35**
trichloroacetic acid	0.7	39	0.087	1.12
formic acid	3.75	13	0.029	0.37
benzoic acid	4.2	31	0.072	0.92
acetic acid	4.76	45	0.105	1.35
pivalic acid	5.03	30	0.064	0.82
/	/	34	0.078	1.00

Computational Methodology

Periodic DFT-D calculations are performed with the Vienna Ab Initio Simulation Package (VASP 5.2.12)[1-4]. The unit cell of all structures is first optimized with a plane wave kinetic energy cutoff of 600 eV, employing the PBE exchange-correlation functional [5,6] with D3-dispersion corrections according to Grimme[7]. Furthermore, the energy cut off of 600 eV is maintained for the energy refinements and frequency calculations. The projector augmented wave approximation (PAW) [8] is used and Brillouin zone sampling is restricted to the Γ-point. Gaussian smearing [2] is applied to improve convergence: 0.05 eV for cell optimizations, 0.02 eV for the subsequent energy and frequency calculations. Furthermore, the convergence criterion for the electronic self-consistent field (SCF) problem is set to 10^{-6} eV while all atomic forces are converged below 0.02 eV/Å during cell optimizations and below 0.01 eV/Å for subsequent energy calculations.

All geometries are built with ZEOBUILDER[9] from the crystallographic information file provided by Cavka et al.[10]. In order to determine free-energy differences between reactants and products in the periodic model, a partial hessian is constructed for that part of the periodic cell which is submitted to changes between the structures of reactants and products. The remaining part of the unit cell is kept fixed. Next, we performed a partial Hessian vibrational analysis (PHVA) [11-15] which was applied previously for modeling of kinetics[16-18]. The numerical partial Hessian is calculated by displacements in *a*, *b* and *c*-axis of ±0.015 Å, while the vibrational modes are extracted using the normal mode analysis as implemented in the in-house developed post-processing toolkit TAMKIN [19].

The unit cell of the parent periodic UiO-66 structure[10] comprises: $\langle Zr_6O_4(OH)_4(BDC)_6\rangle_4$, where BDC^{2-} stands for terephthalate. For convenience the notation $RCOO^-$ is introduced representing half a terephthalate linker. 4 carboxylate oxygen atoms are bound to each Zr atom. For the present calculation, we use a unit cell in which one trifluoroacetate and one defect site are incorporated instead of a terephthalate linker. ; the UiO-66-TFA unit cell is then composed of $\langle Zr_6O_4(OH)_4(RCOO)_{11}(CF_3COO)\rangle$, $\langle Zr_6O_5(OH)_3(RCOO)_{11}\rangle$ and $\langle Zr_6O_4(OH)_4(RCOO)_{12}\rangle_2$.

The Gibbs reaction free energy differences were calculated starting from the cluster $\langle Zr_6O_4(OH)_4(RCOO)_{11}(CF_3COO)\rangle$, at the activation conditions (320 °C, 10^{-3} mbar).

Loss of water from the initial cluster:

$$Zr_6O_4(OH)_4(RCOO)_{11}(CF_3COO) \rightarrow Zr_6O_5(OH)_2(RCOO)_{11}(CF_3COO) + H_2O \qquad (1)$$

$$\Delta G_r = -74.6 \text{ kJ mol}^{-1}$$

Loss of CF_3COOH from the initial cluster:

$Zr_6O_4(OH)_4(RCOO)_{11}(CF_3COO) \rightarrow Zr_6O_5(OH)_3(RCOO)_{11} + CF_3COOH$ (2)

$\Delta G_r = + 24.7$ kJ mol^{-1}

Loss of CF_3COOH from the partially dehydrated cluster from reaction (1):

$Zr_6O_5(OH)_2(RCOO)_{11}(CF_3COO) \rightarrow Zr_6O_6(OH)(RCOO)_{11} + CF_3COOH$ (3)

$\Delta G_r = + 2.9$ kJ mol^{-1}

Theory shows that initially, a partial dehydroxylation (1) is energetically more favourable than the removal of TFA (2). However, from the partially dehydroxylated UiO-66/TFA, the removal of TFA (3) becomes more competitive.

References

(1) Kresse, G.; Furthmuller, J. *Physical Review B* **1996**, *54*, 11169.
(2) Kresse, G.; Furthmuller, J. *Computational Materials Science* **1996**, *6*, 15.
(3) Kresse, G.; Hafner, J. *Physical Review B* **1993**, *47*, 558.
(4) Kresse, G.; Hafner, J. *Physical Review B* **1994**, *49*, 14251.
(5) Perdew, J. P.; Burke, K.; Ernzerhof, M. *Physical Review Letters* **1996**, *77*, 3865.
(6) Perdew, J. P.; Burke, K.; Ernzerhof, M. *Physical Review Letters* **1997**, *78*, 1396.
(7) Grimme, S.; Antony, J.; Ehrlich, S.; Krieg, H. *J Chem Phys* **2010**, *132*.
(8) Blochl, P. E. *Physical Review B* **1994**, *50*, 17953.
(9) Verstraelen, T.; Van Speybroeck, V.; Waroquier, M. *Journal of chemical information and modeling* **2008**, *48*, 1530.
(10) Cavka, J. H.; Jakobsen, S.; Olsbye, U.; Guillou, N.; Lamberti, C.; Bordiga, S.; Lillerud, K. P. *J Am Chem Soc* **2008**, *130*, 13850.
(11) Ghysels, A.; Van Speybroeck, V.; Verstraelen, T.; Van Neck, D.; Waroquier, M. *Journal of Chemical Theory and Computation* **2008**, *4*, 614.
(12) Ghysels, A.; Van Speybroeck, V.; Pauwels, E.; Van Neck, D.; Brooks, B. R.; Waroquier, M. *Journal of Chemical Theory and Computation* **2009**, *5*, 1203.
(13) Ghysels, A.; Van Speybroeck, V.; Pauwels, E.; Catak, S.; Brooks, B. R.; Van Neck, D.; Waroquier, M. *Journal of Computational Chemistry* **2009**, submitted.
(14) Ghysels, A.; Van Neck, D.; Waroquier, M. *Journal of Chemical Physics* **2007**, *127*, 164108.
(15) Ghysels, A.; Van Neck, D.; Van Speybroeck, V.; Verstraelen, T.; Waroquier, M. *Journal of Chemical Physics* **2007**, *126*, 224102.

(16) Lesthaeghe, D.; Van der Mynsbrugge, J.; Vandichel, M.; Waroquier, M.; Van Speybroeck, V. *Chemcatchem* **2011**, *3*, 208.
(17) Van Speybroeck, V.; Van der Mynsbrugge, J.; Vandichel, M.; Hemelsoet, K.; Lesthaeghe, D.; Ghysels, A.; Marin, G. B.; Waroquier, M. *J Am Chem Soc* **2011**, *133*, 888.
(18) Vandichel, M.; Lesthaeghe, D.; Van der Mynsbrugge, J.; Waroquier, M.; Van Speybroeck, V. *J Catal* **2010**, *271*, 67.
(19) Ghysels, A.; Verstraelen, T.; Hemelsoet, K.; Waroquier, M.; Van Speybroeck, V. *Journal of chemical information and modeling* **2010**, *50*, 1736.